Editors' Suggestion

Aharonov-Bohm and Altshuler-Aronov-Spivak oscillations in the quasiballistic regime in phase-pure GaAs/InAs core/shell nanowires

Farah Basarić,[1,2,*] Vladan Brajović,[1,2] Gerrit Behner,[1,2] Kristof Moors,[1,2,†] William Schaarman,[1,2] Andrei Manolescu,[3] Raghavendra Juluri,[4] Ana M. Sanchez,[4] Jin Hee Bae,[1,2] Hans Lüth,[1,2] Detlev Grützmacher,[1,5,2] Alexander Pawlis,[1,5,2] and Thomas Schäpers[1,2,‡]

[1]*Peter Grünberg Institut (PGI-9), Forschungszentrum Jülich, 52425 Jülich, Germany*
[2]*JARA-Fundamentals of Future Information Technology, Jülich-Aachen Research Alliance, Forschungszentrum Jülich and RWTH Aachen University, 52425 Jülich, Germany*
[3]*Department of Engineering, Reykjavik University, Menntavegur 1, IS-102 Reykjavik, Iceland*
[4]*Department of Physics, University of Warwick, Coventry CV4 7AL, United Kingdom*
[5]*Peter Grünberg Institut (PGI-10), Forschungszentrum Jülich, 52425 Jülich, Germany*

(Received 12 March 2025; revised 16 June 2025; accepted 17 July 2025; published 1 August 2025)

The realization of various qubit systems based on high-quality hybrid superconducting quantum devices is often achieved using semiconductor nanowires. For such hybrid devices, a good coupling between the superconductor and the conducting states in the semiconductor wire is crucial. GaAs/InAs core/shell nanowires with an insulating core and a conductive InAs shell fulfill this requirement, since the electronic states are strongly confined near the surface. However, maintaining a good crystal quality in the conducting shell is a challenge for this type of nanowire. In this work, we present phase-pure zinc-blende GaAs/InAs core/shell nanowires and analyze their low-temperature magnetotransport properties. We observe pronounced magnetic flux quantum periodic oscillations, which can be attributed to a combination of Aharonov-Bohm and Altshuler-Aronov-Spivak oscillations. From the gate and temperature dependence of the conductance oscillations, as well as from supporting theoretical transport calculations, we conclude that the conducting states in the shell are in the quasiballistic transport regime, with few scattering centers, but nevertheless leading to an Altshuler-Aronov-Spivak correction that dominates at small magnetic field strengths. Our results demonstrate that phase-pure zinc-blende GaAs/InAs core/shell nanowires represent a very promising alternative semiconductor-nanowire-based platform for hybrid quantum devices.

DOI: 10.1103/xljl-s1lp

I. INTRODUCTION

Semiconductor nanowires are considered to be a versatile building block for various applications in nanoelectronics and quantum devices [1]. In particular, when combined with superconductors, they provide a flexible platform for various applications in classical and topological quantum computing [2–7]. In many cases bulk InAs nanowires are used, since the Fermi level pinning at the surface naturally leads to an accumulation layer at the interface in the semiconductor [8]. This ensures conductive channels even at low temperatures. The accumulation layer also provides good coupling to metallic contacts, which is particularly important in the case of superconducting electrodes. Even better coupling is expected when the electronic state in the nanowire is confined close to the interface with the superconductor by using a semiconductor heterostructure in a core/shell nanowire.

In a core/shell nanowire, the heterointerface between the high-band-gap core semiconductor and the low-band-gap shell material, creating a band offset, forms a radial quantum well that confines the electron wave function close to the outer radius. This results in a tubular conductor [9–12]. Applying an axial magnetic field leads to magnetic flux quantum h/e-periodic Aharonov-Bohm-type (AB) oscillations in the magnetoconductance [13], where e is the electron charge and h is Planck's constant. Aharonov-Bohm-type oscillations have been observed in GaAs/InAs [14–17], GaAs/InSb [18], as well as In_2O_3/InO_x core/shell nanowires [19]. The tubular quantum states in semiconductor core/shell nanowires have certain similarities to the tubular topologically protected surface states in a topological insulator nanowire [20–22]. For this type of nanowire, AB oscillations in the quasiballistic regime have recently been observed. A possible reason for reaching the quasiballistic regime in this case is that spin-momentum locking in topological insulators leads to reduced scattering [23,24]. On the other hand, Altshuler-Aronov-Spivak (AAS) oscillations with a period of $h/2e$ resulting from interference of time-reversed paths have been observed here as well [25], indicating the presence of scattering.

*Contact author: f.basaric@fz-juelich.de
†Present address: Imec, Kapeldreef 75, 3001 Leuven, Belgium.
‡Contact author: th.schaepers@fz-juelich.de

Recently, we have succeeded in growing GaAs nanowires with a phase-pure crystal structure by dynamically controlled growth using molecular beam epitaxy (MBE) [26]. In this study, we use this approach to grow zinc-blende phase-pure GaAs/InAs core/shell nanowires and investigate their transport properties. Due to the phase purity in the InAs shell, we expect significantly reduced scattering in electronic transport. Such a defect-free core/shell GaAs/InAs nanowire growth approach represents a strong advantage over current technological limitations regarding the topological insulator nanowires. This makes it a promising platform for investigation of potentially superior transport properties via crystal phase control with respect to previous studies. Even though our nanowires do not contain inherent topological properties, by covering them with a full-shell superconductor, topological superconductivity might be obtained [27,28]. In this regime of reduced scattering we investigate magnetotransport oscillations that are known to appear in both (quasi)ballistic and diffusive regimes. We carry out in-plane magnetoconductance measurements that give an insight into the characteristics of the transversal mode of transport. Gate-dependent low-temperature transport measurements allow us to disentangle different contributions to the oscillatory behavior of the magnetoconductance. The relevant transport regime is determined by temperature-dependent measurements. We interpret the experimental results by comparing them with transport calculations based on linear response theory (Kubo formalism) and the Landauer formalism (quantum transport simulations using KWANT) [29].

II. EXPERIMENTAL DETAILS

The GaAs/InAs core/shell nanowires are grown by MBE via self-catalyzed vapor-liquid-solid technique on prestructured substrates. To obtain a phase-pure crystal structure, the catalyst droplet on top of the growing nanowires is dynamically controlled during the growth, following the approach reported in Jansen *et al.* [26]. In our case, we achieved a contact angle of the Ga catalyst droplet above 125° resulting in a zinc-blende (ZB) crystal structure. We used Si(111) substrates covered with about 20 nm of thermally deposited SiO_2 containing hole arrays with varying diameters of 40, 60, and 80 nm and pitches with varying pinhole sizes of 0.5, 1, 2, and 4 μm, prepared by electron beam lithography and subsequent dry and wet etching. The GaAs core is grown by applying an As flux with a beam equivalent pressure (BEP) of 5×10^{-6} mbar for 90 min at about 610 °C, while the Ga flux is dynamically decreased by 40% from the starting value of 1.5×10^{-7} mbar. Subsequently, the InAs shell growth is performed at a substrate temperature of 450 °C comprising In and As fluxes with BEPs of 1.95×10^{-7} mbar and 5×10^{-6} mbar, respectively.

In this work, measurements are discussed on three samples, originating from two separate growth runs. In the case of samples A and B the total growth time of 25 min for the InAs shell resulted in a smaller shell thickness t_{shell} compared to sample C with a shell growth time of 40 min (cf. Table I). Figure 1(a) corresponds to a low-magnification annular dark field scanning transmission electron image (ADF-STEM) of the nanowire cross section, i.e., along the ⟨111⟩ direction.

TABLE I. Geometric dimensions and phase-coherence length of samples A to C, where r_{core} denotes the GaAs core radius, t_{shell} the InAs shell thickness, r_{tot} the total nanowire radius, L_c the inner contact separation, and l_φ the phase-coherence length obtained at 1.5 K.

Sample	r_{core} (nm)	t_{shell} (nm)	r_{tot} (nm)	L_c (nm)	l_φ (μm)
A	51	28	79	400	3.3
B	58	27	85	400	2.7
C	56	39	95	450	4.6

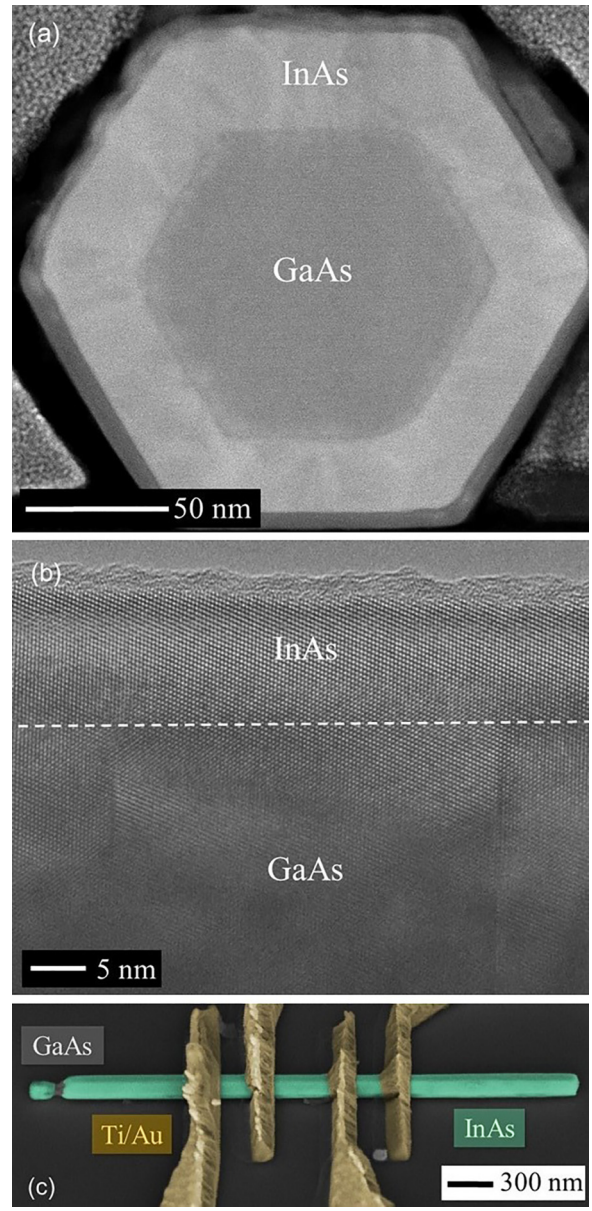

FIG. 1. (a) ADF-STEM image of the GaAs/InAs core/shell nanowire cross section of sample B along the growth direction. (b) High-resolution TEM image of the middle part of a core/shell nanowire. (c) False-color SEM image of a contacted GaAs/InAs nanowire, corresponding to sample A.

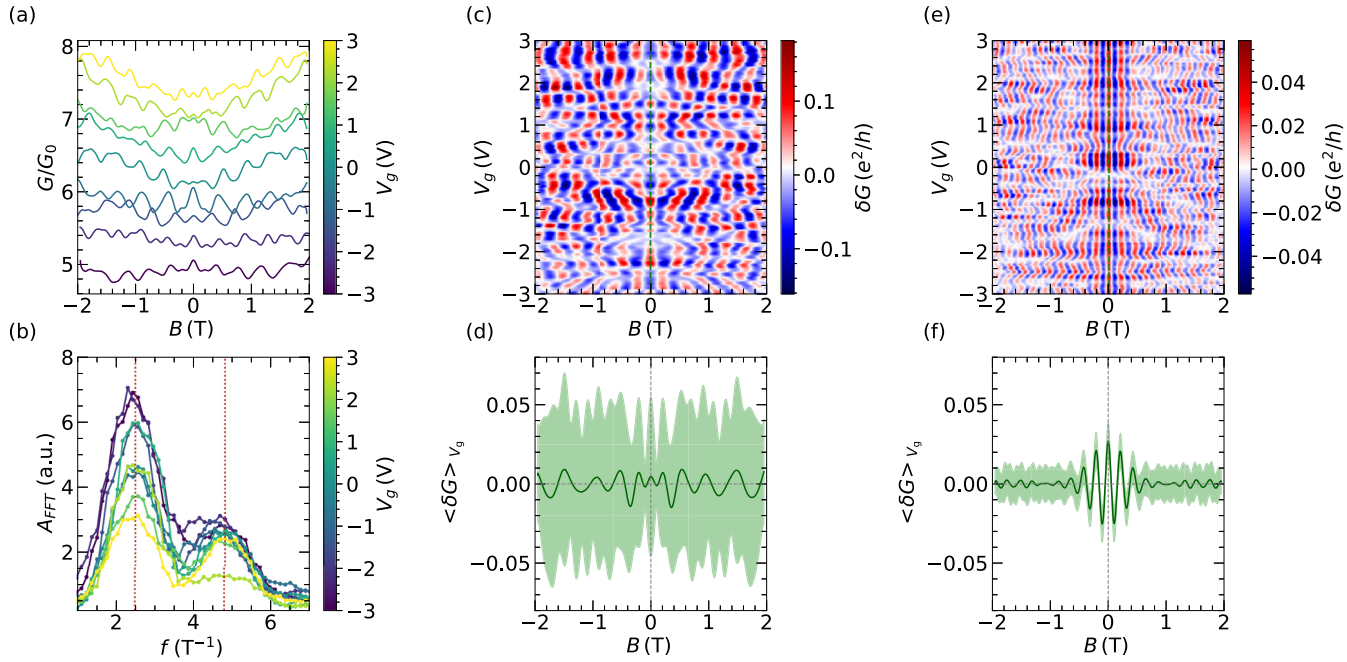

FIG. 2. (a) Normalized conductance G/G_0 of sample A, with $G_0 = e^2/h$, as a function of the magnetic field, displayed for some values of applied gate voltage at 1.5 K, and oscillating with a period of 0.4 T. (b) Fast Fourier transform of the magnetoconductance oscillations shown in (a) featuring a two-peak structure, corresponding to h/e- and $h/2e$-periodic oscillation frequencies at 2.5 and 4.8 T^{-1}, respectively. (c) Color map of filtered-out h/e-periodic conductance contribution as a function of B and V_g. It reveals a nonrigid phase with varying V_g over the entire magnetic field range. (d) Oscillating h/e conductance contribution averaged over the gate voltage range $\langle \delta G \rangle_{V_g}$. The light green area shows the standard deviation. (e) Analogous color-map analysis for $h/2e$-periodic contribution to the one shown in (c). It shows phase rigidity at a small magnetic field range between −0.3 and 0.3 T. (f) Averaged $h/2e$-periodic conductance contribution and standard deviation as in the case of (d).

Figure 1(b) shows a high-resolution TEM image along the ⟨110⟩ direction. This type of image confirmed that ZB crystal structure is the preferred polytype both in the core and the shell. Detailed information on the growth procedure and the crystal structure is given in the Supplemental Material [30].

For the low-temperature transport experiments, the GaAs/InAs core/shell nanowires are transferred by a scanning electron microscope (SEM)–based micromanipulator to a prepatterned Si(100) substrate covered with 150 nm of SiO_2. Employing the precise nanowire transferring technique, as well as the electron beam lithography step and Ar^+ cleaning, the metallization of Ti/Au contact fingers was realized. An example of a measured device is given in Fig. 1(c). As previously mentioned, the measurement results of samples A and C are described here, with additional data from a second nanowire of the first growth run (sample B) summarized in the Supplemental Material [30]. The corresponding geometric dimensions of these nanowires are given in Table I.

The measurements were carried out in a variable temperature insert cryostat, with a base temperature of 1.5 K. Using a four-terminal measurement configuration and a standard lock-in setup, as well as applying an axial magnetic field, the devices were biased with a current of 20 nA between the two outer contacts, whereas the voltage drop was measured between the two inner ones. The contact resistances were on the order of 500 Ω. The inner contact separation L_c for the investigated samples is given in Table I. The highly doped Si substrate was used as a global back gate with the SiO_2 layer used as a gate dielectric.

III. RESULTS AND DISCUSSION

A. Gate dependence

First, we focus on the gate-dependent magnetotransport properties of sample A (the corresponding measurements and analyses of samples B and C are given in the Supplemental Material [30]). The measurements were conducted at 1.5 K in an axial magnetic field. A gate voltage V_g ranging between −3 and 3 V, with a stepping of 0.05 V, was applied to the global back gate. As shown in Fig. 2(a), the normalized magnetoconductance G/G_0, with $G_0 = e^2/h$, reveals regular AB-type oscillations over the entire gate voltage range, where the ring geometry supporting such oscillations was still preserved even at the applied gate voltage of −3 V, and no effects of inhomogeneous gating were thus observed.

From the oscillation period ΔB, the effective area S enclosed by the closed-loop wave function can be determined by the relation $\Phi_0 = \Delta B \times S$, where $\Phi_0 = h/e$ is the magnetic flux quantum. Assuming a hexagonal nanowire cross section, the area is given by $S = r^2(3\sqrt{3}/2)$, where r is the circumradius of the hexagon that is enclosed by the closed-loop wave function. For the extracted period of $\Delta B = 0.4$ T, we get a radius of $r = 56$ nm, confirming that the wave function is located within the InAs shell.

Aharonov-Bohm oscillations are related to a periodic modulation of the average occupation of the phase-coherent conducting states with different quantized transverse momenta enveloping the core [14]. The occupation modulations and thus the conductance oscillations are symmetric under

magnetic field reversal. By shifting the Fermi level position with the gate voltage, the average occupation is forming either a local maximum or a local minimum at $B = 0$, giving rise to phase jumps as a function of the gate voltage between $\theta = 0$ and π in the magnetoconductance oscillation pattern: $\delta G(\phi) \propto \cos[\phi + \theta(V_g)]$, with $\phi = \Phi/\Phi_0$ the normalized magnetic flux and $\theta(V_g)$ the gate-voltage-dependent phase of the oscillation pattern [14]. Note that the average occupation and the corresponding phase in the magnetoconductance oscillation pattern can vary over different parts of the sample under the change of local electron density in an environment of randomly distributed scattering centers within the InAs shell.

To further analyze the experimental data, a fast Fourier transform (FFT) of the magnetoconductance oscillations is performed. Before applying the FFT, the slowly varying background $\overline{G}$ in the experimental data was subtracted from the measured conductance, resulting in an oscillation signal $\delta G = G - \overline{G}$. As can be seen in Fig. 2(b), the FFT spectrum obtained from measurements at different gate voltages systematically shows a two-peak structure. The first peak can be assigned to the AB oscillations with a period of h/e while the second, smaller peak corresponds a period of $h/2e$. The latter can originate from both AAS-type conductance oscillations or higher-harmonic contributions of the AB oscillations. The AAS oscillations result from interference of time-reversed paths in a tubular conductor [31,32].

To gain a deeper insight into the physical origin of the two quantum transport contributions, we analyzed and compared the phase rigidity of the h/e- and $h/2e$-periodic oscillations. For this purpose, the inverse Fourier transform of δG was evaluated. Furthermore, we isolated specific frequency windows in the Fourier spectrum corresponding to the peaks belonging to periods of h/e and $h/2e$, respectively. Such an analysis is shown in Fig. 2(c) for the h/e-periodic oscillations, revealing a complex oscillation pattern with a nonrigid phase as V_g changes. Since the h/e contribution dominates the oscillation pattern, the phase jumps along $B = 0$ follow the phase jumps in the raw data. As a consequence of the random phase shifts with V_g, the conductance averaged over the gate voltage $\langle \delta G \rangle_{V_g}$ basically cancels out while at the same time the standard deviation is very large, as can be seen in Fig. 2(d). The $h/2e$ oscillations, corresponding to the second peak in the FFT spectrum, are not clearly visible in the raw data, i.e., in Fig. 2(a), due to the dominance of h/e-periodic oscillations. However, these oscillations are resolved in the inverse FFT spectrum shown in Fig. 2(e). Interestingly, in a field range between -0.3 and 0.3 T, the $h/2e$-periodic oscillations are phase rigid with a conductance maximum at zero field. Beyond this range the phase rigidity is weakened and eventually lost. The extent of the phase stability can also be deduced from Fig. 2(f), which shows the $h/2e$ conductance oscillations averaged over the entire gate voltage range $\langle \delta G \rangle_{V_g}$. It can be seen that $\langle \delta G \rangle_{V_g}$ has its maximum value at $B = 0$ and then decreases continuously with increasing field, disappearing completely at about ± 0.6 T. The small standard deviation in this range underlines the claim of phase stability, as can be seen in Fig. 2(f). We attribute the phase-rigid part to AAS oscillations. In terms of their rigidity while changing V_g, AAS oscillations are robust to averaging since they originate from interference of time-reversed paths in our tubular InAs shell, as already resolved for polymorphic GaAs/InAs nanowires [14]. The conductance maximum at zero field indicates the presence of spin-orbit coupling due to the weak antilocalization effect [33]. Such a conductance maximum has also been observed in bulk InAs nanowires [34].

The phase rigidity of the $h/2e$-periodic oscillation amplitude up to about ± 0.3 T [cf. Fig. 2(e)] can be explained by the finite thickness of the InAs shell and the corresponding loss of phase matching along the inner and outer radius when an axial magnetic field is applied. Using the approach outlined in Mur *et al.* [35], we obtained a limit of 0.17 T for our shell cross section. This value is in relatively good agreement with the experimentally observed one. Beyond this magnetic field limit, the phase relation of the time-reversed paths is randomized [36,37]. At larger field strengths, the randomized phase relation suppresses the amplitude of $h/2e$ oscillations, which can include higher-harmonic contributions of the h/e AB oscillations as well. As a consequence phase rigidity is lost.

Several features of the experimentally observed oscillations can be reproduced by transport calculations based on linear response theory using the Kubo formalism [38]. This is demonstrated in Fig. 3(a) , which shows the corresponding calculations of the magnetoconductance. The calculations were performed for the cross-sectional dimensions of sample A for different chemical potentials in the expected range of GaAs/InAs nanowires of similar dimensions [14,16]; i.e., for our simulations we assumed a range between 26 and 38 meV. The Zeeman effect was included with a g factor of -14.9 [39]. The general oscillation pattern as well as the phase jumps as a function of chemical potential are well reproduced. Furthermore, by changing the chemical potential, the phase of the oscillations switches. This is in agreement with the experimental results, since applying a gate voltage results in a shift of the chemical potential. However, Kubo formalism assumes an infinite wire length with included disorder. In this approach, the disorder is modeled as a system of uniformly distributed point scatterers, within the self-consistent Born approximation, as summarized in the Supplemental Material [30]. For the applied disorder potential of 0.18 meV, we obtain oscillation amplitudes comparable to the experimental ones, although the total conductance is somewhat larger. Note that higher-order conductance corrections, represented by vertex or Cooperon diagrams, which are important to capture quantum interference effects, and in particular AAS oscillations, are not contained in our calculations. Thus, possible second-harmonic features solely originate from the AB effect, due to discrete variation of the number of transverse channels when the magnetic field increases, the finite thickness of the tubular shell, or its noncircular (hexagonal) cross section.

In order to include the AAS effect in the modeling, tight-binding quantum transport simulations were performed using the software package KWANT [29]. In fact, by this, a regime can be explored, where the transport is governed by a finite number of scattering centers, being the appropriate scenario for our phase-pure nanowires. For the tight-binding description of the core/shell nanowire, a hexagonal cross section corresponding to sample A and a wire length of 4 μm was considered. We chose a long-range potential with

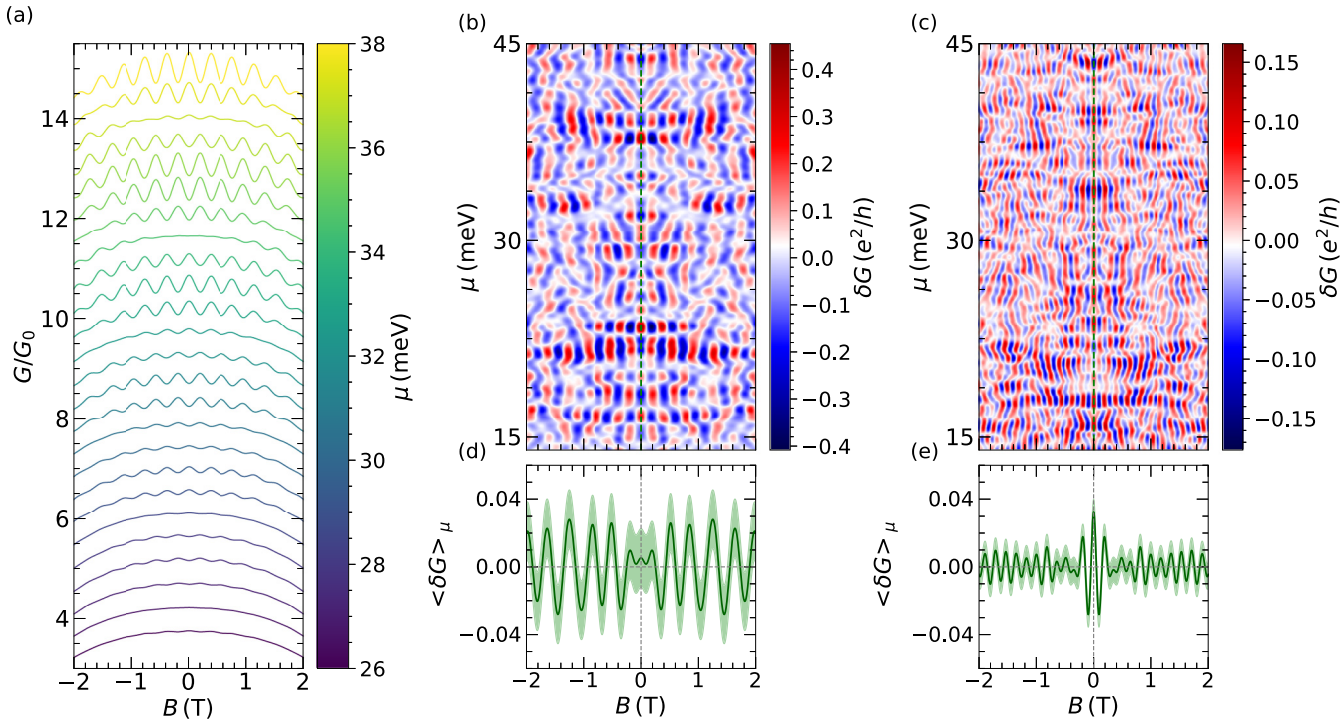

FIG. 3. (a) Normalized magnetoconductance using the Kubo formalism for various values of the chemical potential for a disorder potential of 0.18 meV at 1.5 K. (b) Filtered h/e conductance contribution as a function of B and chemical potential μ of a 4 μm long wire with a disorder potential of 5 meV at 1.5 K, calculated using KWANT package. The geometrical dimensions correspond to sample A. (c) Corresponding filtered $h/2e$-periodic oscillations. (d) Averaged oscillation amplitude $\langle \delta G \rangle_\mu$ over four different disorder potential configuration sets shown by a dark green line, and corresponding standard deviation shown in green. (e) Corresponding averaged oscillation amplitude $\langle \delta G \rangle_\mu$ and standard deviation for the $h/2e$-periodic contribution.

a correlation length slightly smaller than the distance between the leads to represent a system with a few scattering centers along the transport length. More information about the model design can be found in the Supplemental Material [30]. For a direct comparison with the experimental values shown in Figs. 2(c) and 2(d), the filtered first and second harmonics of the simulated conductance are plotted in Figs. 3(b) and 3(c), as a function of magnetic field B and chemical potential μ at a temperature of 1.5 K. The simulations reproduce the general features of the experimentally obtained results; i.e., the oscillation amplitude is lower than in the ideal ballistic case. This can be explained by chemical potential fluctuations due to the presence of scattering centers resulting in fluctuations of the angular momentum state occupation and by that to an averaging of the AB oscillations with different phases along the nanowire. Additionally, we find that the h/e oscillations are non-phase-rigid, whereas the $h/2e$ oscillations largely preserve phase rigidity around zero magnetic field. Furthermore, due to the implemented spin-orbit coupling in the simulations, a maximum of δG is found at zero field. To further support our reasoning, three additional simulations with different disorder configurations were performed. The results of each of these simulations are presented in the Supplemental Material [30]. Figures 3(d) and 3(f) show the conductance oscillations $\langle \delta G \rangle_\mu$ averaged over the chemical potential as a function of magnetic field of the h/e and $h/2e$ periodic contribution, respectively. Each set is averaged over the chemical potential μ, and presented with the standard deviation. The average over the h/e oscillations shows that the signal is significantly damped due to the phase changes with the chemical potential, and the standard deviation extends over a relatively large range. This indicates that the average phase for the four configurations differs to a large degree. In contrast, we find a different behavior for the averaged $h/2e$-periodic conductance contribution, as shown in Fig. 3(f). A clear peak is observed at $B = 0$, consistent with phase-rigid AAS oscillations and the presence of spin-orbit coupling. Although a peak at $B = 0$ is also observed for the h/e oscillations, it does not correspond to robust phase rigidity. This can be seen from the large standard deviation of the $\langle \delta G \rangle_\mu$ pattern and the oscillation amplitude being much lower as compared to the typical oscillation patterns for fixed chemical potential. Interestingly, phase rigidity (associated with a maximum at zero field) was obtained only by considering the full length of 4 μm of the nanowire, whereas by assuming a voltage probe separation of 400 nm, i.e., the separation of the inner contacts, only a random phase is found. We attribute this behavior to the fact that in the case of the 400 nm wire length, the number of scattering centers is too small to result in a sufficient number of time-reversed paths. It effectively means that the entire wire length is probed. Such a nonlocal transport effect is more commonly observed in mesoscopic conductors, which allow an extended region of the wire defined by l_φ (defined in the context of the longitudinal transport mode) to be probed regardless of the relatively small distances of the voltage probes [40]. Summarizing these results, it appears that AAS oscillations show up in our measurements and simulations, which are usually attributed to higher-order

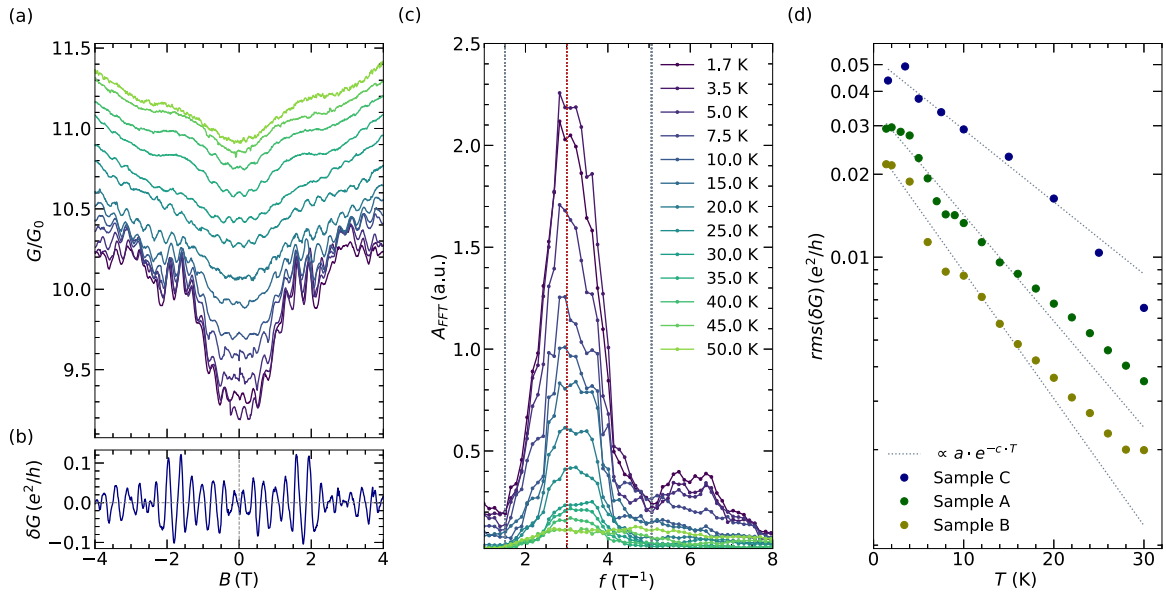

FIG. 4. (a) Temperature-dependent normalized conductance G/G_0 under an axial magnetic field for sample C. (b) Extracted oscillation pattern after subtracting the slowly varying background signal as a function of magnetic field at 1.7 K. (c) Fast Fourier transform of the temperature-dependent measurement shown in (a). The red line marks the peak central position, associated with radius of enclosed wave function within the InAs shell. The gray lines indicate the bounds of the shell. (d) Root mean square (rms) of the Aharonov-Bohm oscillation amplitude as a function of temperature for the three measured samples and corresponding quasiballistic exponential fit. The raw data for samples A and B are offset for clarity by 0.01 e^2/h.

scattering processes, despite the fact that the wire probably has a small number of scattering centers due to the phase purity of the crystal. However, detailed analysis of the nonlocal transport effect remains beyond the scope of the current work.

B. Temperature dependence

In this section, temperature-dependent magnetoconductance measurements for sample C are presented, whereas detailed corresponding descriptions for samples A and B are given in the Supplemental Material [30]. Such measurement gives us a valuable insight into transversal transport mode quality, as well as the value of the phase-coherence length. Figure 4(a) shows the normalized magnetoconductance G/G_0 as the temperature was varied from 1.7 to 50.0 K. Because of the different cross section of sample C compared to A, here we find magnetoconductance oscillations, with a period of $\Delta B = 0.35$ T. The oscillations are superimposed on slower varying conductance modulations, corresponding to universal conductance fluctuations [41]. With increasing temperature, the number of inelastic scattering events increases due to phonon contribution, resulting in a reduction of the phase-coherence length l_φ. This is manifested in a gradual decrease of the oscillation amplitude with rising temperature until they are completely suppressed at around 45.0 K. Figure 4(b) shows the oscillation pattern at 1.7 K after subtracting the slowly varying background signal. The oscillation amplitude is found to be on the order of $0.1e^2/h$, indicating that the longitudinal transport is not fully ballistic but rather quasiballistic. In theoretical calculations it was indeed found that introducing a few scattering centers results in a damping of the oscillation amplitude [10]. The beating pattern observed here is attributed to the effect of Zeeman splitting, which causes spin-dependent shifts in the flux parabolas of the energy spectrum [10].

The periodic features in the magnetoconductance are analyzed in detail by applying an FFT, as presented in Fig. 4(c). The FFT shows a clear peak at a frequency f of about 3.0 T^{-1}, corresponding to the extracted oscillation period given above. The frequency peak indicated by the red dashed line lies within the frequency limits given by the area defined by the inner and outer bounds of the InAs shell. Note that a peak belonging to the second-harmonic frequency at about 6.0 T^{-1} is also observed. With increasing temperature, the peak amplitudes decreases, corresponding to a reduction in the oscillation amplitude. At about 45.0 K the peak is completely suppressed.

An essential insight into the phase-coherent transport of phase-pure core/shell GaAs/InAs nanowires under an in-plane magnetic field is provided by the temperature dependence of the h/e-periodic oscillation amplitude [17]. To resolve it, the slowly varying background was first subtracted from the measured conductance, resulting in an oscillation signal δG, where the average oscillation amplitude is determined by the root mean square rms(δG). Such analysis was carried out for all three samples, and Fig. 4(d) shows the best fit for temperature dependence of rms(δG). From this, it is possible to determine the phase-coherence length l_φ, considering an exponential decay $\mathrm{rms}(\delta G) \propto \exp(-2\pi r/l_\varphi)$ [42]. For all samples, the resulting dependence can be fitted well to the data with $l_\varphi \sim T^{-1}$, i.e., electron-electron scattering [43]. The exponential decay of the h/e-periodic oscillation amplitude suggests a quasiballistic mesoscopic transport regime [44]. Even though the experimental data at higher temperature seem to deviate from this fit, it still is the best representation for all three of our samples. We found no indications for

electron-phonon scattering. Here, we compared between models that describe either the diffusive or quasiballistic transport regime, with or without thermal broadening. This is further displayed and discussed individually for each sample in the Supplemental Material [30]. The obtained dependence is in contrast to previous measurements on core/shell GaAs/InAs nanowires, where a dependence $l_\varphi \sim T^{-p}$ with p of about 0.6 was extracted [17], which is close to the diffusive case [45]. We attribute the different behavior to the improved crystal quality of the present nanowires. From the fit, we determined l_φ at base temperature for each sample (cf. Table I). As expected for the ballistic case, l_φ exceeds the length of the ringlike tubular conductor arm and is found to be significantly larger than previously reported for GaAs/InAs nanowires [17]. Additionally, it is in good agreement with the proposed superior transport properties of phase-pure core/shell nanowires. A quasiballistic transport regime has also been observed in topological nanowire structures, where spin-momentum locking is assumed to be responsible for the reduced scattering [23,24,46].

IV. CONCLUSIONS

In conclusion, phase-coherent transport is studied in phase-pure zinc-blende GaAs/InAs core/shell nanowires. Pronounced Aharonov-Bohm oscillations with a period of h/e are observed. These oscillations arise from the presence of coherent closed-loop states in the InAs shell, which are periodically modulated when a magnetic flux is threaded through the wire cross section. In contrast to previous studies, the temperature dependence of the oscillation amplitude indicates that the transport takes place in the quasiballistic regime. When the electron concentration is varied by a back-gate voltage, the phase of the h/e-periodic oscillations is found to be non-phase-rigid, which is attributed to the lack of time-reversal symmetry of this interference process. Interestingly, the $h/2e$ oscillation component contains a phase-rigid region around zero magnetic fields. This can be explained in the framework of Althshuler-Aronov-Spivak oscillations, where time-reversal symmetry is preserved. It is noteworthy that these oscillations are observed in the quasiballistic regime and not, as usual, in the diffusive regime. At larger magnetic fields, only the second harmonic of the Aharonov-Bohm oscillations remains. The findings on the presence or absence of phase rigidity of the $h/2e$-periodic oscillations are confirmed by quantum transport simulations, where a relatively small number of scattering centers, represented by a disorder potential with a correlation length of 50 nm, are found to conform to the quasiballistic regime and still give rise to phase-rigid Altshuler-Aronov-Spivak oscillations near zero field. However, observation of these oscillations reveals a necessity for further experiments that would clarify its switching mechanism, as well as its correlation to the longitudinal transport properties. The phenomena and the transport regime observed here are very similar to experiments on topological insulator nanoribbons, despite the absence of spin-momentum locking in our case. The quasiballistic transport behavior in our nanowires confirms the expected superior quality of the phase-pure crystal structure, which is highly relevant for the reproducible definition of confined quantum states. The results obtained here are also important for future superconductor/semiconductor nanowire hybrid structures, e.g., for topological [47–49] or Andreev-level qubits [4–6,50]. An important aspect in this context is the coupling of the superconducting shell with the electron gas at the interface, which is favorably achieved by confining the electron system in the shell. In fact, when coupled to a superconducting contact, enhanced magnetoconductance oscillations with a period of $h/2e$ are observed, which are attributed to phase-coherent resonant Andreev reflections [51]. More recently, $h/2e$ oscillations have been found in the switching current of Josephson junctions based on GaAs/InAs core/shell nanowires [52]. In light of these recent experiments, we believe that phase-pure semiconductor nanowires present a very interesting new research direction toward optimization of such hybrid devices.

ACKNOWLEDGMENTS

We thank Herbert Kertz for technical assistance. Dr. Florian Lentz and Dr. Stefan Trellenkamp are gratefully acknowledged for their help with the required e-beam lithography. The sample fabrication has been performed in the Helmholtz Nano Facility at Forschungszentrum Jülich [53]. This work was partly funded by Deutsche Forschungsgemeinschaft (DFG, German Research Foundation) under Germany's Excellence Strategy–Cluster of Excellence Matter and Light for Quantum Computing (ML4Q) EXC 2004/1–390534769. K.M. acknowledges financial support by the Bavarian Ministry of Economic Affairs, Regional Development and Energy, within Bavaria's High-Tech Agenda Project "Bausteine für das Quantencomputing auf Basis topologischer Materialien mit experimentellen und theoretischen Ansätzen" (Grant No. 07 02/686 58/1/21 1/22 2/23) and by the German Federal Ministry of Education and Research (BMBF) via the Quantum Future project "MajoranaChips" (Grant No. 13N15264) within the funding program Photonic Research Germany. A.M.S. and R.J. acknowledge the support of EPSRC Grant No. EP/W002418/1.

DATA AVAILABILITY

The data that support the findings of this article are openly available [54].

[1] G. Badawy and E. P. A. M. Bakkers, Electronic transport and quantum phenomena in nanowires, Chem. Rev. **124**, 2419 (2024).

[2] G. de Lange, B. van Heck, A. Bruno, D. J. van Woerkom, A. Geresdi, S. R. Plissard, E. P. A. M. Bakkers, A. R. Akhmerov, and L. DiCarlo, Realization of microwave quantum circuits using hybrid superconducting-semiconducting nanowire Josephson elements, Phys. Rev. Lett. **115**, 127002 (2015).

[3] T. W. Larsen, K. D. Petersson, F. Kuemmeth, T. S. Jespersen, P. Krogstrup, J. Nygård, and C. M. Marcus,

Semiconductor-nanowire-based superconducting qubit, Phys. Rev. Lett. **115**, 127001 (2015).

[4] L. Tosi, C. Metzger, M. F. Goffman, C. Urbina, H. Pothier, S. Park, A. L. Yeyati, J. Nygård, and P. Krogstrup, Spin-orbit splitting of Andreev states revealed by microwave spectroscopy, Phys. Rev. X **9**, 011010 (2019).

[5] C. Metzger, S. Park, L. Tosi, C. Janvier, A. A. Reynoso, M. F. Goffman, C. Urbina, A. Levy Yeyati, and H. Pothier, Circuit-QED with phase-biased Josephson weak links, Phys. Rev. Res. **3**, 013036 (2021).

[6] P. Zellekens, R. Deacon, P. Perla, D. Grützmacher, M. I. Lepsa, T. Schäpers, and K. Ishibashi, Microwave spectroscopy of Andreev states in InAs nanowire-based hybrid junctions using a flip-chip layout, Commun. Phys. **5**, 267 (2022).

[7] A. Yazdani, F. von Oppen, B. I. Halperin, and A. Yacoby, Hunting for Majoranas, Science **380**, eade0850 (2023).

[8] S. Wirths, K. Weis, A. Winden, K. Sladek, C. Volk, S. Alagha, T. E. Weirich, M. von der Ahe, H. Hardtdegen, H. Lüth, N. Demarina, D. Grützmacher, and T. Schäpers, Effect of Si-doping on InAs nanowire transport and morphology, J. Appl. Phys. **110**, 053709 (2011).

[9] Y. Tserkovnyak and B. I. Halperin, Magnetoconductance oscillations in quasiballistic multimode nanowires, Phys. Rev. B **74**, 245327 (2006).

[10] T. O. Rosdahl, A. Manolescu, and V. Gudmundsson, Spin and impurity effects on flux-periodic oscillations in core-shell nanowires, Phys. Rev. B **90**, 035421 (2014).

[11] G. Ferrari, A. Bertoni, G. Goldoni, and E. Molinari, Cylindrical two-dimensional electron gas in a transverse magnetic field, Phys. Rev. B **78**, 115326 (2008).

[12] A. Manolescu, G. A. Nemnes, A. Sitek, T. O. Rosdahl, S. I. Erlingsson, and V. Gudmundsson, Conductance oscillations of core-shell nanowires in transversal magnetic fields, Phys. Rev. B **93**, 205445 (2016).

[13] Y. Aharonov and D. Bohm, Significance of electromagnetic potentials in the quantum theory, Phys. Rev. **115**, 485 (1959).

[14] O. Gül, N. Demarina, C. Blömers, T. Rieger, H. Lüth, M. I. Lepsa, D. Grützmacher, and T. Schäpers, Flux periodic magnetoconductance oscillations in GaAs/InAs core/shell nanowires, Phys. Rev. B **89**, 045417 (2014).

[15] C. Blömers, T. Rieger, P. Zellekens, F. Haas, M. I. Lepsa, H. Hardtdegen, O. Gül, N. Demarina, D. Grützmacher, H. Lüth, and T. Schäpers, Realization of nanoscaled tubular conductors by means of GaAs/InAs core/shell nanowires, Nanotechnology **24**, 035203 (2013).

[16] F. Haas, T. Wenz, P. Zellekens, N. Demarina, T. Rieger, M. Lepsa, D. Grützmacher, H. Lüth, and T. Schäpers, Angle-dependent magnetotransport in GaAs/InAs core/shell nanowires, Sci. Rep. **6**, 24573 (2016).

[17] F. Haas, P. Zellekens, T. Wenz, N. Demarina, T. Rieger, M. I. Lepsa, D. Grützmacher, H. Lüth, and T. Schäpers, Anisotropic phase coherence in GaAs/InAs core/shell nanowires, Nanotechnology **28**, 445202 (2017).

[18] P. Zellekens, N. Demarina, J. Janßen, T. Rieger, M. I. Lepsa, P. Perla, G. Panaitov, H. Lüth, D. Grützmacher, and T. Schäpers, Phase coherent transport and spin-orbit interaction in GaAs/InSb core/shell nanowires, Semicond. Sci. Technol. **35**, 085003 (2020).

[19] M. Jung, J. S. Lee, W. Song, Y. H. Kim, S. D. Lee, N. Kim, J. Park, M.-S. Choi, S. Katsumoto, H. Lee, and J. Kim, Quantum interference in radial heterostructure nanowires, Nano Lett. **8**, 3189 (2008).

[20] H. Peng, K. Lai, D. Kong, S. Meister, Y. Chen, X.-L. Qi, S.-C. Zhang, Z.-X. Shen, and Y. Cui, Aharonov-Bohm interference in topological insulator nanoribbons, Nat. Mater. **9**, 225 (2010).

[21] S. Cho, B. Dellabetta, R. Zhong, J. Schneeloch, T. Liu, G. Gu, M. J. Gilbert, and N. Mason, Aharonov-Bohm oscillations in a quasi-ballistic three-dimensional topological insulator nanowire, Nat. Commun. **6**, 7634 (2015).

[22] Y. C. Arango, L. Huang, C. Chen, J. Avila, M. C. Asensio, D. Grützmacher, H. Lüth, J. G. Lu, and T. Schäpers, Quantum transport and nano angle-resolved photoemission spectroscopy on the topological surface states of single Sb_2Te_3 nanowires, Sci. Rep. **6**, 29493 (2016).

[23] J. Ziegler, R. Kozlovsky, C. Gorini, M.-H. Liu, S. Weishäupl, H. Maier, R. Fischer, D. A. Kozlov, Z. D. Kvon, N. Mikhailov, S. A. Dvoretsky, K. Richter, and D. Weiss, Probing spin helical surface states in topological HgTe nanowires, Phys. Rev. B **97**, 035157 (2018).

[24] D. Rosenbach, K. Moors, A. R. Jalil, J. Kölzer, E. Zimmermann, J. Schubert, S. Karimzadah, G. Mussler, P. Schüffelgen, D. Grützmacher, H. Lüth, and T. Schäpers, Gate-induced decoupling of surface and bulk state properties in selectively-deposited Bi_2Te_3 nanoribbons, SciPost Phys. Core **5**, 017 (2022).

[25] H.-S. Kim, T.-H. Hwang, N.-H. Kim, Y. Hou, D. Yu, H.-S. Sim, and Y.-J. Doh, Adjustable quantum interference oscillations in Sb-doped Bi_2Se_3 topological insulator nanoribbons, ACS Nano **14**, 14118 (2020).

[26] M. M. Jansen, P. Perla, M. Kaladzhian, N. von den Driesch, J. Janssen, M. Luysberg, M. I. Lepsa, D. Grützmacher, and A. Pawlis, Phase-pure wurtzite GaAs nanowires grown by self-catalyzed selective area molecular beam epitaxy for advanced laser devices and quantum disks, ACS Appl. Nano Mater. **3**, 11037 (2020).

[27] S. Vaitiekėnas, G. Winkler, B. van Heck, T. Karzig, M.-T. Deng, K. Flensberg, L. Glazman, C. Nayak, P. Krogstrup, R. Lutchyn *et al.*, Flux-induced topological superconductivity in full-shell nanowires, Science **367**, 6485 (2020).

[28] M. T. Deng, C. Payá, P. San-Jose, E. Prada, C. M. Marcus, and S. Vaitiekėnas, Caroli–de Gennes–Matricon analogs in full-shell hybrid nanowires, Phys. Rev. Lett. **134**, 206302 (2025).

[29] C. W. Groth, M. Wimmer, A. R. Akhmerov, and X. Waintal, Kwant: A software package for quantum transport, New J. Phys. **16**, 063065 (2014).

[30] See Supplemental Material at http://link.aps.org/supplemental/10.1103/xljl-s1lp for experimental details, transmission electron microscopy studies, additional magnetotransport measurements, and modeling.

[31] B. L. Al'tshuler, A. G. Aronov, and B. Z. Spivak, Aharonov-Bohm effect in disordered conductors, JETP Lett. **33**, 94 (1981).

[32] D. Y. Sharvin and Y. V. Sharvin, Magnetic-flux quantization in a cylindrical film of a normal metal, JETP Lett. **34**, 272 (1981).

[33] A. G. Aronov and Y. V. Sharvin, Magnetic flux effects in disordered conductors, Rev. Mod. Phys. **59**, 755 (1987).

[34] S. E. Hernández, M. Akabori, K. Sladek, C. Volk, S. Alagha, H. Hardtdegen, M. G. Pala, N. Demarina, D. Grützmacher, and T. Schäpers, Spin-orbit coupling and phase coherence in InAs nanowires, Phys. Rev. B **82**, 235303 (2010).

[35] L. C. Mur, C. J. P. M. Harmans, and W. G. van der Wiel, Competition between h/e and $h/2e$ oscillations in a semiconductor Aharonov-Bohm interferometer, New J. Phys. **10**, 073031 (2008).

[36] S. L. Ren, J. J. Heremans, S. Vijeyaragunathan, T. D. Mishima, and M. B. Santos, Determination of time-reversal symmetry breaking lengths in an InGaAs interferometer array, J. Phys.: Condens. Matter **27**, 185801 (2015).

[37] C. P. Umbach, C. Van Haesendonck, R. B. Laibowitz, S. Washburn, and R. A. Webb, Direct observation of ensemble averaging of the Aharonov-Bohm effect in normal-metal loops, Phys. Rev. Lett. **56**, 386 (1986).

[38] R. Kubo, Statistical-mechanical theory of irreversible processes. I. General theory and simple applications to magnetic and conduction problems, J. Phys. Soc. Jpn. **12**, 570 (1957).

[39] R. Winkler, *Spin-Orbit Coupling Effects in Two-Dimensional Electron and Hole Systems* (Springer, Berlin, 2003).

[40] C. P. Umbach, P. Santhanam, C. van Haesendonck, and R. A. Webb, Nonlocal electrical properties in mesoscopic devices, Appl. Phys. Lett. **50**, 1289 (1987).

[41] P. A. Lee, A. D. Stone, and H. Fukuyama, Universal conductance fluctuations in metals: Effects of finite temperature, interactions, and magnetic field, Phys. Rev. B **35**, 1039 (1987).

[42] R. Webb, S. Washburn, C. Umbach, F. Milliken, R. Laibowitz, and A. Benoit, The Aharonov-Bohm effect in normal metals-non-ensemble averaged quantum transport, Phys. A (Amsterdam, Neth.) **140**, 175 (1986).

[43] A. E. Hansen, A. Kristensen, S. Pedersen, C. B. Sørensen, and P. E. Lindelof, Mesoscopic decoherence in Aharonov-Bohm rings, Phys. Rev. B **64**, 045327 (2001).

[44] G. Seelig and M. Büttiker, Charge-fluctuation-induced dephasing in a gated mesoscopic interferometer, Phys. Rev. B **64**, 245313 (2001).

[45] T. Ludwig and A. D. Mirlin, Interaction-induced dephasing of Aharonov-Bohm oscillations, Phys. Rev. B **69**, 193306 (2004).

[46] J. Dufouleur, L. Veyrat, A. Teichgräber, S. Neuhaus, C. Nowka, S. Hampel, J. Cayssol, J. Schumann, B. Eichler, O. G. Schmidt, B. Büchner, and R. Giraud, Quasiballistic transport of Dirac fermions in a Bi_2Se_3 nanowire, Phys. Rev. Lett. **110**, 186806 (2013).

[47] Y. Oreg, G. Refael, and F. von Oppen, Helical liquids and Majorana bound states in quantum wires, Phys. Rev. Lett. **105**, 177002 (2010).

[48] R. M. Lutchyn, J. D. Sau, and S. Das Sarma, Majorana fermions and a topological phase transition in semiconductor-superconductor heterostructures, Phys. Rev. Lett. **105**, 077001 (2010).

[49] E. Prada, P. San-Jose, M. W. de Moor, A. Geresdi, E. J. Lee, J. Klinovaja, D. Loss, J. Nygård, R. Aguado, and L. P. Kouwenhoven, From Andreev to Majorana bound states in hybrid superconductor-semiconductor nanowires, Nat. Rev. Phys. **2**, 575 (2020).

[50] A. Zazunov, V. S. Shumeiko, E. N. Bratus, J. Lantz, and G. Wendin, Andreev level qubit, Phys. Rev. Lett. **90**, 087003 (2003).

[51] O. Gül, H. Y. Günel, H. Lüth, T. Rieger, T. Wenz, F. Haas, M. Lepsa, G. Panaitov, D. Grützmacher, and T. Schäpers, Giant magnetoconductance oscillations in hybrid superconductor-semiconductor core/shell nanowire devices, Nano Lett. **14**, 6269 (2014).

[52] P. Zellekens, R. S. Deacon, F. Basaric, R. Juluri, M. D. Randle, B. Bennemann, C. Krause, E. Zimmermann, A. M. Sanchez, D. Grützmacher, A. Pawlis, K. Ishibashi, and T. Schäpers, Flux-periodic supercurrent oscillations in an Aharonov-Bohm-type nanowire Josephson junction, arXiv:2402.13880.

[53] W. Albrecht, J. Moers, and B. Hermanns, HNF-Helmholtz nano facility, J. Large-Scale Res. Facil. **3**, A112 (2017).

[54] F. Basarić, V. Brajović, G. Behner, K. Moors, W. Schaarman, A. Manolescu, R. Juluri, A. M. Sanchez, J. H. Bae, H. Lüth, D. Grützmacher, A. Pawlis, and T. Schäpers, Data for: Aharonov-Bohm and Altshuler-Aronov-Spivak oscillations in the quasi-ballistic regime in phase-pure GaAs/InAs core/shell nanowires, JülichDATA (2025), https://doi.org/10.26165/JUELICH-DATA/D94JMC.